Cronfa - Swansea University Open Access Repository

_____

This is an author produced version of a paper published in:
Phys. Chem. Chem. Phys.

_____

Paper:

_____

http://www.swansea.ac.uk/library/researchsupport/ris-support/

PCCP

Accepted Manuscript

PCCP

Physical Chemistry Chemical Physics
www.rsc.org/pccp

Volume 18 | Number 1 | 7 January 2016 | Pages 1–636

ISSN 1463-9076

ROYAL SOCIETY OF CHEMISTRY

PERSPECTIVE
Darya Radziuk and Helmuth Möhwald
Ultrasonically treated liquid interfaces for progress in cleaning and separation processes

175 YEARS

ROYAL SOCIETY
OF CHEMISTRY

rsc.li/pccp

Resonance Raman and IR spectroscopy of Aligned Carbon Nanotube Arrays with Extremely Narrow Diameters Prepared with Molecular Catalysts on Steel Substrates

Sagar Motilal Jain[a,b], Federico Cesano[b], Domenica Scarano[b] and Tomas Edvinsson[c]*

[a]SPECIFIC, College of Engineering Swansea University Bay Campus, Fabian Way, SA1 8EN Swansea, United Kingdom

[b]Department of Chemistry, NIS (Nanostructured Interfaces and Surfaces) Centre of Excellence and INSTM Centro di Riferimento, University of Torino, Via P. Giuria, 7, 10125 Torino, Italy

[c]Department of Engineering Sciences, Solid State Physics, Uppsala University, Box 534, SE 751 21 Uppsala, Sweden.

Abstract

Carbon nanotubes (CNTs) are considered promising for a large range of emerging technologies ranging from advanced electronics to utilization as nanoreactors. Here we report a controlled facile synthesis of aligned carbon nanotubes with very small dimensions directly grown on steel grid substrate via two-step catalytic chemical vapor deposition (CCVD) of molecular catalyst (Ferrocene) with Ethylene as carbon source. The system is characterized by resonance Raman and show single walled carbon nanotube (SWCNT) arrays composed of 0.80 nm and 1.24 nm semiconducting CNTs, as analyzed with Kataura analysis, approaching the lowest diameters attainable in SWCNTs.

The G^+ and G^- mode splitting, G^+ line shapes, and ring breathing modes (RBMs) are analyzed to characterize the CNTs. The approach results in close packed and vertically aligned SWCNT

bundles formed into a carbon hair shapes, with some contributions from multiwall CNTs (MWCNTs). IR spectroscopy is utilized to characterize the edge/defect states with the possibilities to form esters and ether bonds in the as-prepared CNTs. The stepwise deposition of catalyst followed by carbon source gives a control over formation of small diameter single walled carbon nanotubes (SWCNT). The utilization of molecular catalysts for narrow diameter growth directly on steel grid substrates forms a promising approach for producing cost-effective CNT substrates for a plethora of sensing and catalytic applications.

Keywords: Carbon nanotubes (CNTs), Catalytic Chemical vapour deposition (CCVD), Resonance Raman spectroscopy, Infrared spectroscopy (IR), surface properties.

Carbon nanotubes (CNTs) represent innovative materials for many technological applications due to their interesting properties, coming from the two dimensional (2D) confinement of electronic and phonon states.[1-3] The applications include nanoelectronics, tough composites, functional nanostructured materials, and novel probe microscopy tips,[4-6] where the diameters and the chirality of the CNTs to a large extent determine the properties of the system, such as the metallicity, density of edge states *etc*.[3] The 2D confined nanotubes, corresponding to a 1D material system, are the smallest dimension structures to be used for efficient transport of electrons and optical excitations, where extensive research is made about the nature of transport through 1D systems and how do these properties depend, for example, on diameter and structure.[3]

To this aim, many investigations on the growth and characterization of aligned and patterned CNTs on a variety of flat substrates such as silicon, glass and plastic have been performed.[6-10]

Films with CNT covered substrates may be used in transistors, chemical and flow sensors, electrical contacts, mechanically tuned composites, and catalyst supports.[2, 11-14]

The first low-dimensional CNTs were reported by Iijima 1991 in a fullerene arc discharge reactor using graphite electrodes with the smallest diameter of 2.2 nm,[15] while earlier studies also have reported hollow carbon filaments[16] and also catalyst induced filamentous carbon.[17] Thereafter, many techniques have been developed to synthesize CNTs, such as arc-discharge, laser ablation of graphite and catalytic chemical vapour deposition (CCVD). The Catalysed Chemical Vapour Deposition of CNTs is similar to the general CVD processes, except for the use of metal catalyst. For this reason the process is often referred as catalytic chemical vapour deposition (CCVD). Typically, hydrocarbons are flowing into a preheated furnace at a controlled rate, where they are decomposed by metal catalysts (commonly Fe, Ni or Co) previously deposited on a substrate (e.g. silicon, silica, plastic, glass etc), to produce CNTs.[18] The small clusters, acting as catalyst nuclei, give rise to SWCNTs and MWCNTs. In this work we have systematically exploited the 2 step deposition method for preparation of small diameter carbon nanotubes on steel substrate, where in first step deposited dense (high density) forest of ferrocene catalyst is flown deposited and thermal decomposition of ferrocene provides both catalytic particles and carbon source and in second step Ethylene is used as additional carbon source. Moreover, by controlling the synthesis conditions (temperature, flow rate, time, pressure), the nucleation of larger catalyst particles can be suppressed and high density catalyst formation promoted, thus favoring the formation of nanotubes with smaller diameter.

Raman spectroscopy is a well-established tool for obtaining information without damaging the CNT structure [3, 4] and in particular for determining the degree of structural ordering and the morphology, including the diameter of the tubes or their conductance properties together with the presence of contaminants.[19] The first-order Raman spectra of all graphite-like materials,

including MWCNTs and SWCNTs, show a strong peak around 1580 cm^{-1}, which is the high-frequency E_{2g} first-order mode, whose position is rather independent of excitation wavelengths; it is reported that unlike graphite, the tangential G mode (G-band) of SWCNTs is a sum of several energy tangential modes (~6-8), which originate from breaking the symmetry of the tangential vibration when a graphene sheet is rolled into a tube structure.[4, 20] Among these, two intense modes labeled G^+ and G^-, related to the atomic displacement along the tube axis (G^+) and along the circumferential direction (G^-), have been highlighted, where the shape of G^- mode depends on whether the tube is semiconductor (Lorentzian line shape) or metallic (Breit-Wigner-Fano, BWF line fit).[4, 20, 21] Whereas the G^+-G^- splitting is large for small diameter SWCNTs, the corresponding splitting of the G-band in MWCNTs is small, because of the diameter distributions within individual MWCNTs.[3, 21] A disorder-induced band around 1350 cm^{-1} (D-band) and an high frequency shoulder of the G band around 1620 cm^{-1} (labeled D' or G*), is explained in terms of double resonant Raman scattering due to defective situations.[21]

The shape, the position and the intensity of D-modes, which correspond to the sp^3 – hybridized carbon atoms, are correlated with the extent of the disorder and the defects of graphitic walls and with the laser beam excitation wavelengths.[22]

It can be highlighted that D' band may become more intense than the G band for excitation wavelength in infrared region. The increase of the relative intensity of the D and D' bands (I_D/I_G and ($I_{D'}/I_G$) with excitation wavelengths has already been observed by other authors and it is related to a larger electron–phonon interaction for D and D' bands with respect to G peak, as described by double resonance theory.[19, 20, 23] The presence of G band and the dispersive behavior (i.e. the frequency shift with the excitation frequency) of D and D' bands, together with the band widths give information on the graphitization degree of the materials.[3]

Additional features in the radial breathing mode (RBM) region (350-100 cm^{-1}) are due to the

presence of different nanotubes, simultaneously in resonance with the laser photon frequency.

The Raman-active radial breathing modes (R band) are sensitive to the nanotube diameter,

which in turn depend on the chirality of the CNTs. From the chirality vector C_k, defined in Fig

1, and the carbon-carbon bond-length (a_{c-c}), and simply utilizing that the perimeter is $C_k = \pi \cdot d_t$,

the tube diameter (d_t) can be expressed as

$$d_t = \frac{C_k}{\pi} = \frac{\sqrt{3}a_{c-c}}{\pi}\sqrt{m^2 + nm + n^2} \tag{1}$$

By utilizing that each component in the RBM band has a frequency given by the equation[19]

$$\omega_{RBM} = \frac{C_1}{d_t} + C_2 \tag{2}$$

where ω is the vibration frequency, d_t is the tube diameter in nm and the empiric parameters C_1

and C_2, one can obtain the chirality vector from RBM analysis form Raman spectroscopy. In our

case, 234 cm^{-1}nm and 10 cm^{-1} are used for C_1 and C_2, respectively, to obtain natural number

multiples in the analysis. The chosen values for other systems, however, are depending on the

set of expected multiples which in turn depend on the nanotubes present (metallic or

semiconducting) as well as on possible intertube interactions.[21] Analysis of the geometric

construction of the different chiralities in SWNTs show that if the difference between n and m is

divisible with three, i.e. *(n-m)=3J* where J is a natural number, one of the possible sub-bands

intersect the *K* point in reciprocal space and thus makes the system metallic. The band gap of

the 2/3 of the CNTs that are semiconducting can be quite easily estimated due to the close to

linear dispersion of energies with *k* close to the Fermi level, E$_F$, in graphene. The energy gap

between the states closest to K is directly proportional to Δk between the sub-bands, where Δk is

only dependent on the graphene width, that is *Ck* in Fig 1. Since Ck is directly related to the

diameter of the tube (Eq 1), regardless of the precise combination of n and m, the band gap is

only dependent on the diameter of the tube. For SWCNTs larger that about 1 nm, strain induced

shifts of electronic states at room temperature can be neglected and the band gap can be

estimated by a parameterized equation; $Eg=(0.85 \text{ eVnm})/d_t$ where a 1 nm and 2 nm SWCNT

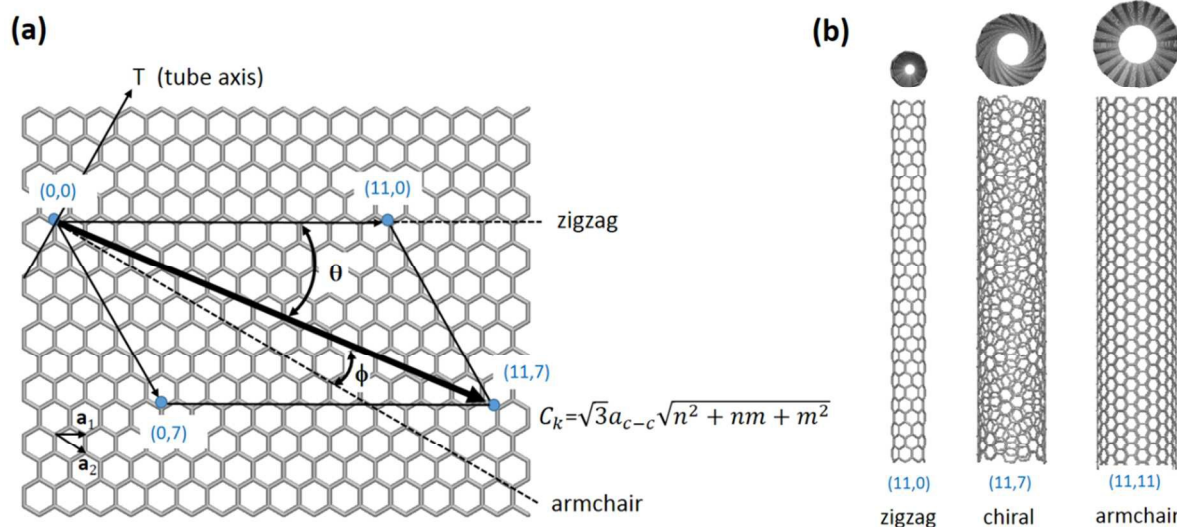thus would give a bandgap of 0.85 eV, and 0.43 eV respectively.

Fig 1. (a) Illustration and definition of the chiral vector C_k (m,n) and the relation to the zigzag (n=0), armchair (m=n), and tube axis (T) directions. (b) Zigzag, chiral and armchair CNTs with indices as defined from (a).

Raman scattering, although providing a powerful tool to obtain CNTs chirality and dimensions

via the nanotube phonons and optical excitations, it is not able to detect all relevant functional

groups adsorbed on the CNT walls or interior relevant to the surface reactivity and scaffolding

properties. Infrared spectroscopy is here a complementary tool, keeping in mind that IR activity

of carbonaceous materials with covalent bond character show very low intensities and can be

difficult to characterize.[24, 25] Adsorption bands are often very broad, artifacts can appear and a

good dilution/dispersion with inert matter can be necessary. With respect to more polar bonds,

however, IR spectroscopy have a relevant role for analysis of bonding to oxygen and defects at

the surface.

The knowledge of morphology, dimensions, chirality and surface defectiveness of CNTs, well

dispersed on suitable supports, can help in understanding the nature of CNTs-biological

molecule interactions[26, 27] as well as for application in sensing and catalysis. In this context, the

properties of the "as-prepared" carbon nanotubes films have also been investigated by means of

scanning electron microscopy (SEM) and IR spectroscopy. The IR spectra are also compared

with those of the included reference materials (commercial SWCNTs and MWCNTs).

A photo and SEM/AFM images of the CNTs grown on the metal grid are shown in **Fig 2**. The

iron catalyzed decomposition of ethylene into carbon gives rise to a dense network of carbon

nanotubes on the grid (**Fig 2**a), whose cavities appear completely covered at the end of the

process (**Fig 2**b). Exploded view at a different level of magnification of a selected small area

(**Fig 2**c) show aligned and closed packed filaments, which are elongated along a preferential

direction (cross-section view of CNTs, region 1), with CNT bundles (top-view of packed CNTs,

region 2) ranging in the 40÷100 nm interval (**Fig 2**d). Strong accumulated van der Waals (vdW)

forces along the carbon nanotubes are considered to be responsible for strong driving force for

packing individual CNTs into aligned CNT bundles (**Fig 2**e). Isolated nanotubes deposited on

HOPG, as obtained after unbundling the high-density CNT network (i.e. sonication in IPA),

have been AFM imaged (**Fig 2**f). The measured heights clearly indicate that the majority of

SWCNTs have small diameters (~ 0.8-1.6 nm) (**Fig 2**g, height profiles 1 and 2), although a

small fraction of larger nanotubes and MWCNTs is also evidenced (**Fig 2**g, height profile 3).
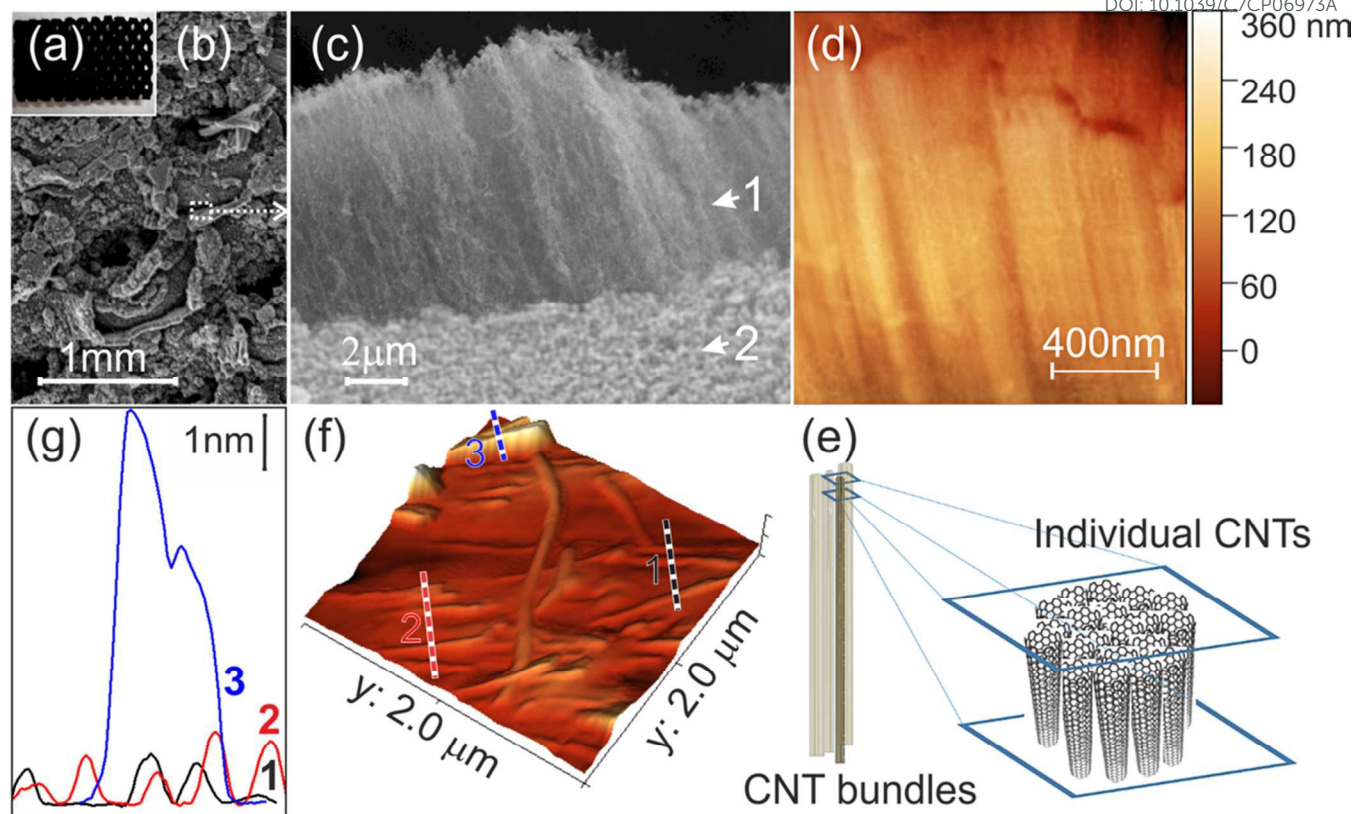
Fig 2. Picture (a), top-view SEM image (b), selected-area micrograph (c) and AFM image (d) of the aligned CNTs covering the steel grid; (e) illustration of the van der Waals aggregated individual CNTs into filament bundles; 3D AFM image (f) and height profile along the selected lines (1, 2 and 3) (g) of the same CNTs deposited on HOPG. Regions 1 and 2 in (c) evidence cross-section and top-views view of the oriented CNT bundles.

Raman spectra of the synthesized CNTs and of two reference materials (SWCNTs and MWCNTs) was acquired at room temperature using 514 nm and 785 nm laser excitations (**Fig 3**a,b). The Raman spectrum obtained using 514 nm of the as grown CNTs (**Fig 3**a, black line) shows two distinctive regions corresponding to: the G-band, at 1583 cm^{-1} and the D-band, at 1354 cm^{-1} (defect mode)[4, 28-31] (**Fig 3**a. black line).

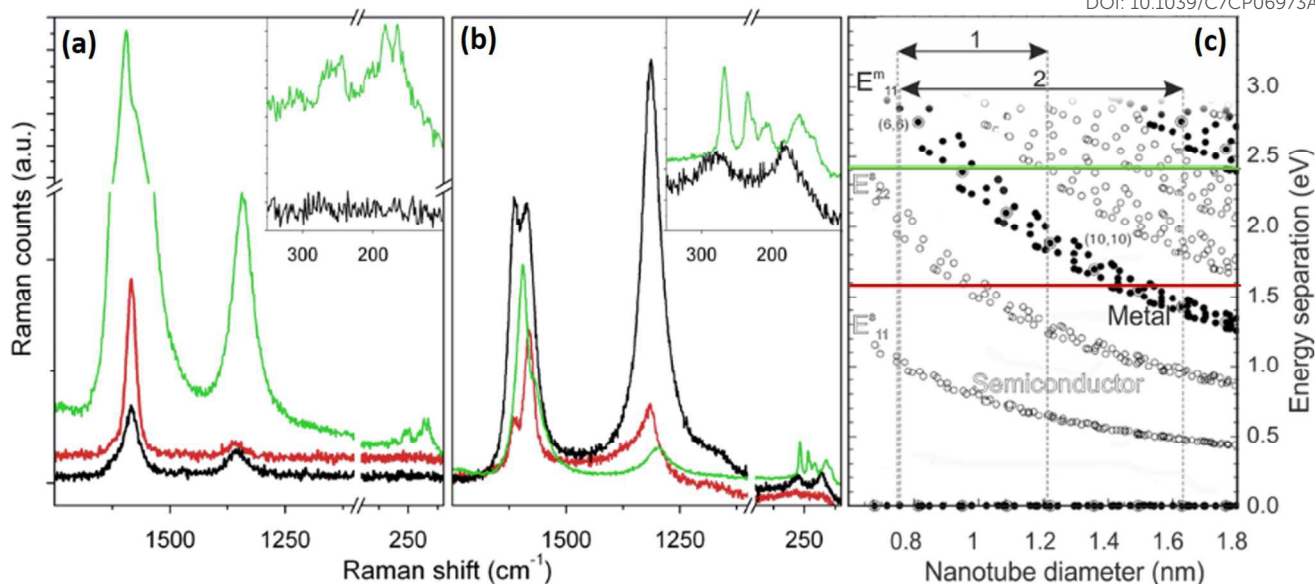**Fig 3.** Raman spectra using the (a) 514 nm and (b) 785 nm laser lines, showing G, D and RBM bands of the as grown CNTs (black line), as compared to the commercial MWCNTs (red line) and SWCNTs (green line). (c) Kataura plot [32] showing resonance excitations (E_{nn}) as function of nanotube diameters. Horizontal green and red lines refer to laser energies with 532 nm and 785 nm, respectively.

The G- and the D-bands of the commercial samples, obtained under 514 nm excitation, are placed at 1582 cm^{-1} and at 1352 cm^{-1} (MWCNTs, red line) and at 1597 cm^{-1} (with a shoulder at 1568 cm^{-1}) and at 1341 cm^{-1} (SWCNTs, green line). Notice that, the G-band of the SWCNTs (green line in **Fig 3**a) is asymmetric and the frequency values of the as grown CNTs are slightly higher than those of reference MWCNTs, but lower than those of SWCNTs.

The 785 nm laser excitation is commonly adopted to better highlight sample defects, as it is confirmed from the better resolved vibrational features in the Raman spectra (**Fig 3**b). The G-band of the as grown CNTs (**Fig 3**b, black line) is composed by two distinct peaks with maxima at 1615 cm^{-1} (before assigned to D' or G* bands), whereas the D-band is placed at 1313 cm^{-1}.

An overall observation shows that the D band downshifts with increasing wavelength and its relative intensity increases, in agreement with the very strong D line observed in Raman spectra

of aligned carbon nanotubes.[33] The same can be observed for the D' band at 1615 cm^{-1} already explained in terms of double resonant Raman scattering due to defective situations.

Concerning the two reference materials, the G band peaks at 1581 cm^{-1} with a shoulder at 1615 cm^{-1} and the D band at 1323 cm^{-1} (MWCNTs, **Fig 3**b, red line). The band at 1596 cm^{-1}, with a shoulder at 1563 cm^{-1}, can be assigned to the G^+- G^- features, and the D band at 1298 cm^{-1} (SWCNTs, **Fig 3**b, green line). It is noteworthy that likewise to the as grown CNTs, although less intense, the spectrum of MWCNTs (**Fig 3**b red line) shows a shoulder at 1615 cm^{-1} (D' band) due to defective situations, unlike SWCNTs (**Fig 3**b green line). In conclusion, by comparing both the sequence of spectra in **Fig 3** a,b, the frequency values of the as grown CNTs are slightly higher than those of reference MWCNTs, and lower than those of reference SWCNTs, inclusion of a portion of MWCNTs in our as prepared samples is likely .

For the as prepared CNTs, the I_G/I_D ratio at 785 nm is reversed (I_G/I_D <1) (with respect to the situation under 514 nm measurements). The defects in graphitic structures are very sensitive to the excitation wavelength, thus causing remarkable variation in the intensity of D and G bands. Conversely, the two reference materials show I_G/I_D >>1. This means that the obtained materials show a higher degree of imperfection with the simultaneous presence of bundles of MWCNTs and SWCNTs. The prepared samples would thus be very suitable for sensing and catalytic applications, while the approach is less suited for advanced electronic applications. Low dimensional CNTs, even if metallic, could be gated with no conductance at low source-drain bias if defected, and thus give rise to pseudo-semi-conducting properties due to defect induced conductance at low gate voltages in the 1D system, but for normal source-drain bias this is more unlikely. Under 514 nm radiation, new features in the radial breathing mode (RBM) region are present (inset in **Fig 3**a, green line) and on the basis of the previously discussed equations, diameters of SWCNTs, comprised in the ~0.84-1.66 nm range, are obtained.[21, 34]

The observed RBM features indicate the simultaneous presence of metallic (with low diameter values) and semiconducting (with higher diameter values) SWCNTs. No RBMs under 514 nm laser line excitation are shown for our sample (inset in **Fig 3**a, black line).

Conversely, at 785 laser excitation, our sample (inset in **Fig 3**b, black line,) is semiconducting in character, shows two distinct wide signals with maxima at $\sim$ 180 cm^{-1} and at $\sim$ 279 cm^{-1}, which corresponds to diameters between 0.80 nm and of 1.24 nm, whereas the well resolved features in the 0.84- 1.60 nm range (insert in **Fig 3**b, green line) can be explained with the simultaneous presence of metallic (higher diameters) and semiconducting (lower diameters) SWCNTs (**Fig 3**c, Fig. S1 and Fig. S2 in the ESI†).

Depending on the diameter, the red or green lasers can excite selectively semiconducting or metallic tubes (resonance Raman).[32] In fact, it is known that the vibrational frequencies in the $\sim$350-100 cm^{-1} range (RBM) are observable only for those nanotubes having the E_{ii} energy close to the laser excitation energies (resonant enhancement) [35] (514 nm=2.41 eV and 785 nm =1.58 eV, in our experiments).

From these results, we can state that the excitation laser line affects the frequency values of D and RBM bands, the I_G/I_D ratio, the G-D bands separation and finally from the obtained results,[35, 36] we can conclude that our sample consists of semiconducting SWCNTs of small diameter ($\approx$0.80$\leq$d$\leq$1.24) together with a portion of MWCNTs. Models of SWCNTs, corresponding to the two maxima (279 cm^{-1} and 180 cm^{-1}) observed in the RBM region of the Raman spectra (inset in **Fig 3**b, green line) with characters of the resulting SWCNTs close to limiting values are summarized in Table 1.

Table 1. Chiral vector (C_k), angle and diameter of the lowest and highest dimensional SWCNTs grown on the steel grids as extracted from analysis of the Raman spectra.

CNT	C_k (m,n)	Chiral angle[a], θ (degrees)	Diameter (nm)	Metallicity[b]	Band gap[c] (eV)
SWCNT	(9,2)	9.8	0.81	S	1.05
	(7,5)	24.5	0.83	S	1.02
	(8,4)	19.1	0.84	S	1.01
	(10,1)	8.4	0.84	M	-
	(11,7)	22.7	1.25	S	0.68
	(14,3)	9.5	1.25	M	-
	(12,6)	19.1	1.26	S	0.67

[a] *Chiral angle as defined from the deviation from the zigzag direction (n=0, Fig 1 (a))*

[b] *Semiconducting (S) and metallic (M)*

[c] *Estimated through the parametrized equation Eg=(0.85 eVnm)/diameter* and neglecting strain.

To investigate the surface properties of CNTs and defects of nanotubes, FTIR spectra of the as prepared CNTs (a) are compared with those of commercial MWCNTs (b) and SWCNTs (c) in **Fig 4**.
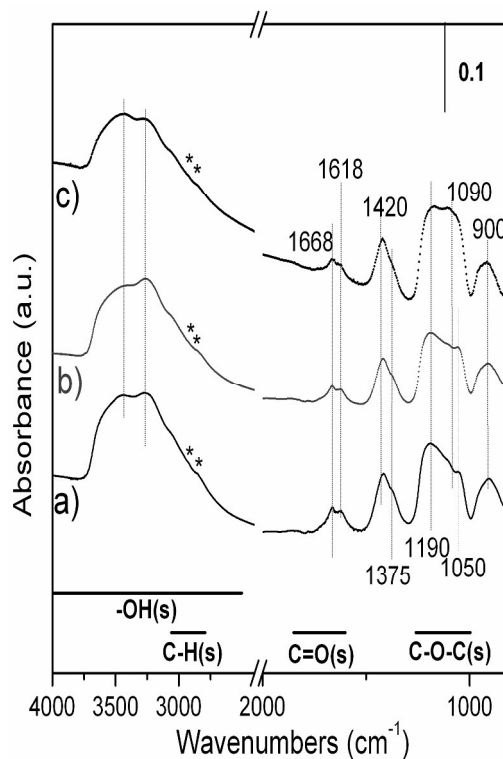
Fig 4. FTIR spectra of (a) as prepared CNTs; (b) commercial MWCNTs; (c) commercial SWCNTs.

All samples show quite similar intense and broad bands in the ~3600-2600 cm^{-1} range, due to the stretching vibrations of a variety of –OH moieties (in carboxyl groups and in –OH shifts in adsorbed water) and to C-H stretching modes of the CH_2 and CH_3 alkyl moieties (marked with asterisks) in the 3000-2800 cm^{-1} interval.[37] The shifts at lower wavenumbers, as compared with isolated –OH moieties, indicate the presence of strong hydrogen bonds between –OH groups.. The bands in the 1650-1600 cm^{-1} range can be attributed to the conjugation of C=C with C=O or the interaction of the skeletal CNT and carboxyl or ketone groups.[37] It is noteworthy that, the coupling of these bands with functionalities containing polar groups can reduce the double bond character of the C=O bond, thus causing the IR bands to downshift.[38]

IR active modes of CNTs can be found in the 1580–1530 cm^{-1} (C-sp^2) and 1200-1100 cm^{-1} (more disordered sp^3 carbon) intervals. Such CNT skeletal vibrational modes depend on the

CNT symmetry and the expected wavenumbers in the IR spectrum are influenced by the nanotube diameters.[37]

The bands in the 1300–900 cm^{-1} range can be assigned to C–O bonds in various chemical surroundings (combination of OH deformation and of C-O stretching modes (e.g. C–O–C groups, oxygen bridges, etc.), together with C-H bending vibrations. Furthermore, absorptions near 1400 cm^{-1} are due to the overlapping of stretching vibrations of $-CH_x$ groups (saturated C-H groups, such as CH_2 and CH_3)[39] with OH in-plane deformations of adsorbed water (OH in-plane deformations).[25, 38, 40] On the basis of the obtained results (high relative intensities and wide separation of bands in the IR region), we can conclude that both the CNTs, produced by the catalytic method and the reference materials (commercial SWCNTs and MWCNTs) show functional groups (-OH, -CH, C-O-C, -C=O), which indicating a relevant surface reactivity.[22] These vibrational characteristics have been observed in native and in purified nanotubes and they progressively increase in intensity upon CNTs functionalization.[26]

Concerning IR-active modes, which are assigned in literature to SWCNTs and MWCNTs, the following should be remarked. IR spectroscopy gives only an indirect picture of the structural properties, while it provide indeed a detailed description of the surface species. Vibrational modes of conjugated C=C bonds (C-sp^2) are for a fact very weak in the IR spectra, because they are not associated with a variation of the dipole moment. Such vibrations can be noticeably detected in the IR spectra in the presence of defects (C-sp^3) located at the periphery of the C-sp^2 domains, thus helping in the modification of the dipole moment.[41] In addition, under the adopted measurement conditions, we are not able to assign the IR features to C-C bonds in the SWCNTs or MWCNTs samples. The dispersion of the samples on KBr pellet, without vacuum annealing, causes the adsorption of a wide amount of impurities, which doesn't allow to distinguish carefully between functional groups formed during the growth process or due to measurements

conditions. Moreover, the intertube interactions (bundling) either the interactions at the surface

of nanotubes, make the separate modes of the SWCNTS and the MWCNTs hard to distinguish.

Nevertheless, Fourier Transform Infrared Spectroscopy can have a role in assigning the surface

functional groups, which together with the vdW attractions are responsible of the observed

bundling phenomena.

The cost of our newly developed single walled carbon nanotubes is almost 4 times cheaper than

the commercial available CNTs from Mitsui and Elicarb that we used in this study (Table S2).

Conclusions

We have demonstrated controlled two step CVD method where the formation of aligned and

patterned mixture of low dimensional SWCNTs and MWCNTs can be achieved by a relatively

simple method, based on CCVD of ethylene on iron coated steel grid substrate using a

molecular catalyst (Ferrocene, $FeCp_2$). SEM images show the formation of a network of aligned

and closed packed filaments on the substrate, which are elongated along a preferential direction

and are hundreds μm in length. Raman spectra of the CCVD grown samples, under 514 nm and

785 laser radiations, together with analysis of the G^+ and G^- mode splitting, G^+ line shapes, and

ring breathing modes (RBMs) show the formation of bundles of semiconducting SWCNTs of

small diameter (0.80≤d≤1.24) together with MWCNTs. IR spectroscopy revealed different

kinds of chemical groups on the surface of CNTs beneficial for further functionalization: from

carbon-hydrogen moieties to oxygen containing functional groups due to the presence of oxygen

trace in ethylene and in the catalyst. The resulting CNTs with narrow diameter grown directly

on steel grid substrates forms a promising system for a plethora of sensing and catalytic applications.

Experimental

CNT synthesis

CNTs were grown on steel grid substrates by a two-step catalytic chemical vapor deposition (CCVD) process. Where first the ferrocene molecular catalyst was evaporated at high temperature and then ethylene gas was introduced as carbon source to boost formation of carbon nanotubes. The synthesis was carried out inside a horizontal tube reactor ($d_{tube} \approx 2.5$ cm) on a sample grid, which is used as a substrate to deposit the catalyst and to grow CNTs. The grid was located in the middle of the quartz tube perpendicular to the flow direction, whereas a small quartz vessel containing $FeCp_2$ (~ 0.5 g) was placed in the cold region of the inlet tube. The highly volatile $FeCp_2$ sublimes at $\sim 170^{o}$ C and starts to decompose at T $\sim 500°$C. Iron clusters and reactive carbon species, which are formed in the gas phase react and move through the reactor. Hence, the grid placed perpendicular to the gas flow direction, together with the hole-shaped geometry of the support (holes of 0.5-1 mm) and the rough morphology of the grid (see Fig S3 in the ESI†) help in increasing the deposition/adhesion of the floating catalyst at the surface of the grid. The temperature of the oven was increased ($\sim 20^{o}$C/min) up to 800°C and stabilized under controlled atmosphere (70 ml/min N_2 gas flow). At 800°C, a mixture of C_2H_4/H_2 (4/1) was flowed (total flow 90 ml/min) for 1h, then the gas flow was switched to N_2 and the temperature reduced.

Commercial CNTs

SWCNTs (Elicarb) were obtained from Thomas Swan and Co. Ltd, United Kingdom. They are high quality single-wall carbon nanotubes, with low inorganic residue (< 5% w/w) and typical nanotube contents of > 90%. Typical nanotube dimensions are smaller than 2 nanometer in diameter and about 1 micron in length.

MWCNT (Mitsui) are high quality multi-wall carbon nanotubes, with very low inorganic residue. Typical nanotube dimensions are 50-70 nanometers in diameter and 10's of microns in length.[30, 31] Ferrocene (98%, Sigma Aldrich) was used as catalyst precursor for the catalytic synthesis of carbon nanotubes.

Characterization Techniques

The as grown CNTs were investigated by vibrational spectroscopies (Raman and IR) and microscopies (SEM and AFM). The Raman spectra were acquired by using a micro–Raman Renishaw spectrometer equipped with a CCD detector. An argon ion laser (514 nm) and a solid state laser (785 nm (red) laser lines were used. All the measurements were performed at room temperature: the commercial reference samples were analyzed in powder form, whereas the as grown CNTs were directly investigated on the supported steel grid.

IR spectra of CNTs were obtained in air at RT in transmission mode (FTIR Bruker IFS-28 spectrometer, equipped with a MCT cryogenic detector. Each IR spectrum was averaged from 128 acquisitions (scan resolution of 4 cm^{-1}) of CNTs deposited on the KBr pellet after dispersion in diethyl ether (0.1 mg/10 ml) and sonication for 10 min.

Scanning electron microscopy images of CNTs, grown on steel grid substrate, were taken on a Zeiss Evo50 SEM instrument operating at 30 kV. AFM images were acquired with a Park XE-100 instrument (SSS-NCL Si probes with tip radius <5nm, NanoSensors) by using an in-house made configuration with a dedicated setup for a very soft interaction to handle delicate

samples.[42] Thus vertically oriented CNTs were imaged along the cross-section of the sample as obtained from the steel grid with a cutter, adhesive tape and then acquired in tapping-mode. Isolated nanotubes, collected from the same CNTs, were imaged on freshly cleaved HOPG after sonication for 15' in isopropyl alcohol (0.1 mg/10 ml) and deposition.

Author Contributions

Dr. S. M. J prepared CNTs, done the FTIR characterization and analysis, plotted the graphs and written the manuscript, Dr. F. C. acquired the SEM and AFM images, participated in preparation of CNTs and participated in writing the manuscript, Prof. D. S. edited the manuscript, Prof T.E. participated in writing and final editing of the manuscript, performed the theoretical assessments and interpretation of the resonance Raman and FTIR spectroscopy.

Acknowledgement

L. J. Ma, J. Liu, L. Deng, M. Zhao, Z. Deng, X. Li, J. Tang and L. Yang, Photochem. Photobiol. Sci., 2014, 13, 1521.

References

1.   M. Y. Sfeir, F. Wang, L. Huang, C.-C. Chuang, J. Hone, S. P. O'brien, T. F. Heinz and L. E. Brus, *Science*, 2004, **306**, 1540.
2.   M. S. Dresselhaus, G. Dresselhaus and P. Avouris, eds., *Carbon Nanotubes: Synthesis, Structure, Properties, and Applications*, Springer-Verlag Berlin-Heidenberg, 2001.
3.   S. Reich, C. Thornsen and J. Maultzsch, eds., *Carbon Nanotubes, Basic Concepts and Physical Properties*, WILEY-VCH Verlag GmbH & CO., Wenheim, 2004.
4.   J. H. Lehman, M. Terrones, E. Mansfield, K. E. Hurst and V. Meunier, *Carbon*, 2011, **49**, 2581.
5.   F. Cesano and D. Scarano, in *Carbon for Sensing Devices*, eds. D. Demarchi and A. Tagliaferro, Springer International Publishing, Switzerland, Heidelberg, New York, Dordrecht, London, 2015, vol. 12, ch. 3, pp. 43.
6.   Z. F. Ren, Z. P. Huang, J. W. Xu, J. H. Wang, P. Bush, M. P. Siegal and P. N. Provencio, *Science*, 1998, **282**, 1105.
7.   S. Hofmann, C. Ducati, B. Kleinsorge and J. Robertson, *Applied Physics Letters*, 2003, **83**, 4661.
8.   G. Haznedar, S. Cravanzola, M. Zanetti, D. Scarano, A. Zecchina and F. Cesano, *Materials Chemistry and Physics*, 2013, **143**, 47.
9.   H. Borchert, F. Witt, A. Chanaewa, F. Werner, J. Dorn, T. Dufaux, M. Kruszynska, A. Jandke, M. Höltig, T. Alfere, J. Böttcher, C. Gimmler, C. Klinke, M. Burghard, A. Mews, H. Weller and J. Parisi, *Journal of Physical Chemistry C*, 2012, **116** 412.
10.   F. Cesano, S. Bertarione, D. Scarano, G. Spoto and A. Zecchina, *Diamond and Related Materials*, 2009, **18**, 979.
11.   H. Kind, J.-M. Bonard, C. Emmenegger, L.-O. Nilsson, K. Hernadi, E. Maillard-Schaller, L. Schlapbach, L. s. Forró and K. Kern, *Advanced Materials*, 1999, **11**, 1285.
12.   D. Srivastava, C. Wei and K. Cho, *Applied Mechanics Reviews*, 2003, **56**, 215.
13.   S. Cravanzola, G. Haznedar, D. Scarano, A. Zecchina and F. Cesano, *Carbon*, 2013, **62**, 270.
14.   F. Cesano, I. Rattalino, F. Bardelli, A. Sanginario, A. Gianturco, A. Veca, C. Viazzi, P. Castelli, D. Scarano and A. Zecchina, *Carbon*, 2013, **61**, 63.
15.   S. Iijima, *Nature*, 1991, **354**, 56.
16.   L. V. Radushkevich and V. M. Lukyanovich, *Zurn. Fisic. Chim.*, 1952, **26**, 88.
17.   R. T. K. Baker, P. S. Harris, R. B. Thomas and R. J. Waite, *J. Catal.*, 1973, **30**, 86.
18.   F. Cesano, S. Bertarione, D. Scarano and A. Zecchina, *Chemistry of Materials*, 2005, **17**, 5119.
19.   E. F. Antunes, A. O. Lobo, E. J. Corat, V. J. Trava-Airoldi, A. A. Martin and C. Veríssimo, *Carbon*, 2006, **44**, 2202.
20.   F. Hennrich, R. Krupke, S. Lebedkin, K. Arnold, R. Fischer, D. E. Resasco and M. M. Kappes, *The journal of physical chemistry. B*, 2005, **109**, 10567.
21.   S. Costa, E. Borowiak-Palen, M. Kruszynska, A. Bachmatiuz and R. J. Kalenkzuk, *Materials Science-poland*, 2008, **26**, 433.
22.   S. Hussain, *Journal of Modern Physics*, 2011, **02**, 538.
23.   R. Saito, A. Grüneis, G. G. Samsonidze, V. W. Brar, G. Dresselhaus, M. S. Dresselhaus, A. Jorio, L. G. Cançado, C. Fantini, M. A. Pimenta and A. G. Souza Filho, *New Journal of Physics Volume*, 2003, **5**, 157.151.
24.   G. I. Dovbeshko, O. P. Gnatyuk, A. N. Nazarov, Y. I. Sementsov and E. D. Obraztsova, eds., *Fullerenes, Nanotubes and Carbon Nanostructures*, Taylor & Francis, Philadelfia, 2005.
25.   U. Kim, X. Liu, C. Furtado, G. Chen, R. Saito, J. Jiang, M. Dresselhaus and P. Eklund, *Physical Review Letters*, 2005, **95**, 157402.
26.   G. I. Dovbeshko, M. Fesenko, E. D. Obraztsova, K. R. Allakhverdiev and A. E. Kaja, *Journal of Structural Chemistry*, 2009, **50**, 954.
27.   D. Gavello, I. Fenoglio, B. Fubini, F. Cesano, F. Premoselli, A. Renna, E. Carbone and V. Carabelli, *NeuroToxicology*, 2013, **39**, 84.
28.   A. Barreiro, S. Hampel, M. H. Rümmeli, C. Kramberger, A. Grüneis, K. Biedermann, A. Leonhardt, T. Gemming, B. Büchner, A. Bachtold and T. Pichler, *The journal of physical chemistry. B*, 2006, **110**, 20973.

29.   G. Cravotto, D. Garella, E. Calcio Gaudino, F. Turci, S. Bertarione, G. Agostini, F. Cesano and D. Scarano, *New Journal of Chemistry*, 2011, **35**, 915.

30.   I. Fenoglio, E. Aldieri, E. Gazzano, F. Cesano, M. Colonna, D. Scarano, G. Mazzucco, A. Attanasio, Y. Yakoub, D. Lison and B. Fubini, *Chemical Research in Toxicology*, 2012, **25**, 74.

31.   D. Gavello, D. Vandael, R. Cesa, F. Premoselli, A. Marcantoni, F. Cesano, D. Scarano, B. Fubini, E. Carbone, I. Fenoglio and V. Carabelli, *Nanotoxicology*, 2012, **6**, 47.

32.   H. Kataura, Y. Kumazawa, Y. Maniwa, I. Umezu, S. Suzuki, Y. Ohtsuka and Y. Achiba, *Synthetic Metals*, 1999, **103**, 2555.

33.   W. Li, H. Zhang, C. Wang, Y. Zhang, L. Xu, K. Zhu and S. Xie, *Applied Physics Letters*, 1997, **70**, 2684.

34.   A. G. Filho Souza, S. Chou, G. Samsonidze, G. Dresselhaus, M. S. Dresselhaus, L. An, J. Liu, K. A. Swan, M. S. Ünlü, B. Goldberg, A. Jorio, A. Grüneis and R. Saito, *Physical Review B*, 2004, **69**, 115428.

35.   A. Jorio, M. A. Pimenta, A. G. Filho Souza, R. Saito, G. Dresselhaus and M. S. Dresselhaus, *New Journal of Physics* 2003, **5**, 139,131.

36.   C. Thomsen, S. Reich and J. Maultzsch, *Philos. Trans. A Math. Phys. Eng. Sci.*, 2004, **362**, 2337.

37.   V. Tucureanu, A. Matei and A. M. Avram, *Critical Reviews in Analytical Chemistry* 2016, **46**, 502.

38.   U. J. Kim, C. a. Furtado, X. Liu, G. Chen and P. C. Eklund, *Journal of the American Chemical Society*, 2005, **127**, 15437.

39.   S. Cravanzola, F. Cesano, F. Gaziano and D. Scarano, *Frontiers in Chemistry*, 2017 accepted, **1**, 1.

40.   L. Stobinski, B. Lesiak, L. Kövér, J. Tóth, S. Biniak, G. Trykowski and J. Judek, *Journal of Alloys and Compounds*, 2010, **501**, 77.

41.   A. Centrone, L. Brambilla, T. Renouard, L. Gherghel, C. Mathis, K. Müllen and G. Zerbi, *Carbon*, 2005, **43**, 1593.

42.   D. Scarano, S. Bertarione, F. Cesano, G. Spoto and A. Zecchina, *Surf. Sci.*, 2004, **570**, 155.